# $R_2Sn_3$ (R = La – Nd, Sm): A Family of Intermetallic Compounds with their Own Triclinic Structure

Maria L. Fornasini[a], Pietro Manfrinetti[b], Andrea Palenzona[b], and Sudesh K. Dhar[c]

[a] Dipartimento di Chimica e Chimica Industriale, Università di Genova, Via Dodecaneso 31, 16146-Genova, Italy
[b] INFM and Dipartimento di Chimica e Chimica Industriale, Università di Genova, Via Dodecaneso 31, 16146-Genova, Italy
[c] CMP & MS, T.I.F.R., Homi Bhabha Road, Mumbai 400 005, India

Reprint requests to M. L. Fornasini. E-mail: cfmet@chimica.unige.it

Z. Naturforsch. **58b,** 521 – 527 (2003); received January 16, 2003

*Dedicated to Prof. A. Iandelli on the occasion of his 90th birthday*

A new family of intermetallic compounds with stoichiometry $R_2Sn_3$ has been identified in the R-Sn system for R = La, Ce, Pr, Nd and Sm. All compounds have a new triclinic crystal structure: $P\overline{1}$, $a = 6.378(1)$, $b = 8.422(1)$, $c = 11.098(1)$ Å, $\alpha = 107.37(1)^\circ$, $\beta = 96.78(1)^\circ$, $\gamma = 100.03(1)^\circ$ for $Nd_2Sn_3$. As a characteristic motif, the structure contains infinite chains of neodymium trigonal prisms centred by tin and sharing alternately a lateral face and an edge of a triangular face.

Heat capacity measurements reveal that the compounds with R = Ce, Pr, Nd and Sm order magnetically and undergo multiple magnetic transitions; from entropy considerations it appears that the four symmetry in-equivalent Ce atoms in $Ce_2Sn_3$ and the Sm atoms in $Sm_2Sn_3$ are all in the trivalent state. The highest transition temperature of nearly 24 K is observed for $Sm_2Sn_3$. The magnetisation and heat capacity data of $La_2Sn_3$ indicate a superconducting transition with a $T_c$ of about 2.5 K.

*Key words:* Crystal Structure, Rare Earth Stannides, Heat Capacity, Magnetic Measurements

## Introduction

Binary rare earth-tin systems have been the object of numerous studies, as reported in the Massalski collection [1]. Moreover, several magnetic properties were investigated [2, 3, and references cited therein]. More recently, the Eu-Sn phase diagram was determined [4] and the results for Yb-Sn revised [5].

However, the high reactivity of these compounds towards moisture and oxygen in the 40 – 70 at.% Sn range prevented, especially for the light R elements, the determination of the whole diagrams and the complete identification of all the occurring phases. Indeed, the composition range going from about 45 at.% Sn ($R_5Sn_4$, $Sm_5Ge_4$-type) to 62.5 at.% Sn ($R_3Sn_5$, $Pu_3Pd_5$-type) still remains the least defined, either in the number of existing compounds or in their structure and composition. Since literature information about light rare earth phases existing in this range are in some cases apparently contradictory, a brief survey will be given.

Phases $R_{11}Sn_{10}$ have been reported for R = La, Ce, Nd and Sm; interestingly no Pr compound with this stoichiometry has been mentioned. For $La_{11}Sn_{10}$ a tetragonal $Ho_{11}Ge_{10}$-type structure was suggested [6], while for $Ce_{11}Sn_{10}$ a structure presumably related to this type with an approximate 11:10 composition [7,8], or an orthorhombic distortion [2] was proposed. According to another work [9], powder patterns of the Nd and Sm homologues are indexed on the basis of the $Ho_{11}Ge_{10}$ type, while the Ce and Pr phases, very close to the 11:10 composition, appear isotypic with each other but with a different structure.

Equiatomic phases RSn are reported to exist only for R = La, Pr and Nd; LaSn forms the orthorhombic CrB-type [6], while the crystal structures for PrSn [10] and NdSn [11] have not been determined.

Formation of compounds with $R_2Sn_3$ composition has been cited only for R = La, Ce, Sm, but no crystal structures have been reported. The existence of $La_2Sn_3$ was derived by thermal effects detected by DTA analyses [6]. A compound "$Ce_2Sn_3$" had been

Table 1. Cell parameters of the $R_2Sn_3$ phases.

| Compound | *a* (Å) | *b* (Å) | *c* (Å) | $\alpha$ (°) | $\beta$ (°) | $\gamma$ (°) | Volume (Å$^3$) | Method |
|---|---|---|---|---|---|---|---|---|
| $La_2Sn_3$ | 6.518(3) | 8.592(7) | 11.296(7) | 107.29(5) | 96.63(4) | 100.32(7) | 584.6(7) | powder |
| $Ce_2Sn_3$ | 6.444(1) | 8.510(2) | 11.195(2) | 107.36(2) | 96.78(2) | 99.42(2) | 567.7(2) | single crystal |
| $Pr_2Sn_3$ | 6.405(1) | 8.452(1) | 11.140(1) | 107.33(1) | 96.76(1) | 99.99(1) | 557.7(1) | single crystal |
| $Nd_2Sn_3$ | 6.378(1) | 8.422(1) | 11.098(1) | 107.37(1) | 96.78(1) | 100.03(1) | 551.0(1) | single crystal |
| $Sm_2Sn_3$ | 6.337(3) | 8.351(6) | 10.995(7) | 108.38(6) | 96.51(6) | 99.99(5) | 534.9(6) | powder |

Table 2. Crystal data of $Nd_2Sn_3$.

| | |
|---|---|
| Pearson code | aP20 |
| Space group | $P\bar{1}$ (No. 2) |
| Temperature, Z | 293 K, 4 |
| Calculated density (g/cm$^3$) | 7.77 |
| Crystal size (mm$^3$) | 0.06×0.08×0.15 |
| Scan mode, $\theta$ range | $\omega - \theta$, 2° −27.5° |
| Range in $h, k, l$ | −8 +8; −10 +10; −14 +14 |
| Total number of reflections | 5027 |
| Absorption coefficient (mm$^{-1}$) | 31.7 |
| Reflections for $\psi$-scan | 3 |
| Transmission ratio (max/min) | 1.83 |
| Independent reflections | 2514 |
| $R_{int}(F_o^2)$ | 0.035 |
| Reflections with $F_o > 4\sigma(F_o)$ | 2097 |
| Number of parameters | 92 |
| Extinction coefficient | 0.00183(9) |
| $wR(F_o^2)$, all data | 0.066 |
| $R[F_o > 4\sigma(F_o)]$ | 0.029 |
| Goodness of fit, S | 1.091 |
| $\Delta\rho_{min}$, $\Delta\rho_{max}$ (e Å$^{-3}$) | −1.91, 1.95 |

Table 3. Atomic coordinates and equivalent isotropic displacement parameters of $Nd_2Sn_3$. $U_{eq}$ is defined as one third of the trace of the orthogonalized $U_{ij}$ tensor.

| Atom | *x* | *y* | *z* | $U_{eq}$(Å$^2$) |
|---|---|---|---|---|
| Nd1 | 0.12497(9) | 0.75434(7) | 0.38415(5) | 0.0118(1) |
| Nd2 | 0.33130(9) | 0.03189(7) | 0.74426(5) | 0.0106(1) |
| Nd3 | 0.55746(9) | 0.43026(7) | 0.33660(5) | 0.0103(1) |
| Nd4 | 0.95756(9) | 0.25128(7) | 0.05628(5) | 0.0111(1) |
| Sn1 | 0.04761(11) | 0.35353(9) | 0.37934(7) | 0.0114(2) |
| Sn2 | 0.17698(12) | 0.03681(9) | 0.22304(7) | 0.0117(2) |
| Sn3 | 0.22233(11) | 0.40567(9) | 0.86456(6) | 0.0107(2) |
| Sn4 | 0.32332(11) | 0.60140(9) | 0.13884(6) | 0.0111(2) |
| Sn5 | 0.35675(12) | 0.16539(9) | 0.49875(7) | 0.0139(2) |
| Sn6 | 0.43750(12) | 0.16965(9) | 0.05187(7) | 0.0128(2) |

mentioned in an early study of the binary phase diagram by Vogel and Heumann [12] but, since not confirmed in subsequent and more recent works, this compound is actually absent in the compilation of phase diagrams [1]. However, on the basis of the work of ref. [12], magnetic measurements on Ce stannides including "$Ce_2Sn_3$" were performed [13]. The $Sm_2Sn_3$ compound was identified by Percheron in a study on the Sm-Sn system [14]; though a tentative tetragonal cell was reported, its crystal structure remained unsolved.

We have reexamined the $R_2Sn_3$ phases with R = La, Ce, Pr, Nd, Sm and this work reports on their crystal structure and some physical properties.

## Experimental Section

Starting materials for the preparation of the stannides were ingots of the commercial pure elements (99.9 wt.% purity for R and 99.999 wt.% for Sn); for the rare earth metals, turnings were freshly prepared by machining under a pure Ar flow. Although the compounds could be prepared by direct melting in arc or induction-heating furnaces of compacted pellets (except for $Sm_2Sn_3$), the use of a sealed Ta crucible proved to be a better way both to obtain larger crystallites and to minimise oxidation. The turnings were mixed and pressed into outgassed Ta crucibles, sealed by welding under pure Ar and melted by induction heating in a high-frequency furnace up to 1250 – 1350 °C (about 150 °C above the liquidus temperature, as taken from ref. [1] and its updates). The containers were then closed under vacuum in quartz tubes and samples subjected to annealing; thermal treatment was carried out in two subsequent steps: first at 1050 °C for 14 days, second at 800 °C for 14 days (900 °C for 21 days and 800 °C for 7 days, for $Sm_2Sn_3$).

X-ray investigations were performed on powders and single crystals. For powder patterns the Debye-Scherrer method was used, with a 114.6 mm diameter camera; powders were prepared by grinding the sample under pure argon and sealed under vacuum in Lindemann capillaries. For single crystal studies, crystals were picked out after crushing grains submerged in low-viscosity perfluoropolyether, sealed under vacuum in oven-dried glass capillaries and checked by Laue photographs. Even after this protective handling, the life time of crystals was only a few days. For the three compounds $Ce_2Sn_3$, $Pr_2Sn_3$ and $Nd_2Sn_3$ single crystals were employed and lattice parameters obtained from 25 diffractometer-measured reflections in the $\theta$ range 24° – 26°. X-ray intensity data of a $Nd_2Sn_3$ single crystal were collected on an Enraf-Nonius CAD-4 diffractometer with graphite-monochromated Mo-K$_\alpha$ radiation. Both $\psi$-scan and spherical absorption corrections were applied. The structure solution was performed by SIR92 [15] and full-matrix least-squares refinement based on $F_o^2$ was made with SHELXL-97 [16] with atomic coordinates standard-

Table 4. Interatomic distances (Å) in $Nd_2Sn_3$.

| | | | | | |
|---|---|---|---|---|---|
| Nd1- | Sn3 | 3.104(1) | Nd2- | Sn6 | 3.205(1) |
| | Sn4 | 3.156(1) | | Sn5 | 3.253(1) |
| | Sn1 | 3.269(1) | | Sn4 | 3.261(1) |
| | Sn5 | 3.280(1) | | Sn3 | 3.263(1) |
| | Sn5 | 3.306(1) | | Sn2 | 3.275(1) |
| | Sn1 | 3.309(1) | | Sn2 | 3.285(1) |
| | Sn2 | 3.372(1) | | Sn1 | 3.476(1) |
| | Sn5 | 3.568(1) | | Sn6 | 3.543(1) |
| | Nd2 | 3.909(1) | | Sn5 | 3.706(1) |
| | Nd3 | 4.010(1) | | Nd1 | 3.909(1) |
| | Nd2 | 4.015(1) | | Nd3 | 3.935(1) |
| | | | | Nd1 | 4.015(1) |
| Nd3- | Sn6 | 3.177(1) | | Nd4 | 4.070(1) |
| | Sn5 | 3.261(1) | | | |
| | Sn3 | 3.282(1) | Nd4- | Sn3 | 3.211(1) |
| | Sn1 | 3.309(1) | | Sn2 | 3.223(1) |
| | Sn4 | 3.315(1) | | Sn4 | 3.235(1) |
| | Sn1 | 3.322(1) | | Sn6 | 3.255(1) |
| | Sn5 | 3.435(1) | | Sn6 | 3.260(1) |
| | Sn2 | 3.527(1) | | Sn3 | 3.287(1) |
| | Sn1 | 3.564(1) | | Sn4 | 3.301(1) |
| | Nd3 | 3.668(1) | | Sn2 | 3.303(1) |
| | Nd2 | 3.935(1) | | Sn1 | 3.380(1) |
| | Nd1 | 4.010(1) | | Sn6 | 3.740(1) |
| | | | | Nd2 | 4.070(1) |

Table 4 (continued).

| | | | | | |
|---|---|---|---|---|---|
| Sn1- | Sn2 | 3.024(1) | | | |
| | Sn5 | 3.143(1) | Sn2- | Sn5 | 2.934(1) |
| | Sn1 | 3.254(2) | | Sn6 | 2.998(1) |
| | Nd1 | 3.269(1) | | Sn1 | 3.024(1) |
| | Nd1 | 3.309(1) | | Nd4 | 3.223(1) |
| | Nd3 | 3.309(1) | | Nd2 | 3.275(1) |
| | Nd3 | 3.322(1) | | Nd2 | 3.285(1) |
| | Nd4 | 3.380(1) | | Nd4 | 3.303(1) |
| | Nd2 | 3.476(1) | | Nd1 | 3.372(1) |
| | Nd3 | 3.564(1) | | Nd3 | 3.527(1) |
| Sn3- | Sn4 | 2.913(1) | Sn4- | Sn3 | 2.913(1) |
| | Sn4 | 2.927(1) | | Sn3 | 2.927(1) |
| | Nd1 | 3.104(1) | | Nd1 | 3.156(1) |
| | Nd4 | 3.211(1) | | Nd4 | 3.235(1) |
| | Nd2 | 3.263(1) | | Nd2 | 3.261(1) |
| | Nd3 | 3.282(1) | | Nd4 | 3.301(1) |
| | Nd4 | 3.287(1) | | Nd3 | 3.315(1) |
| | Sn4 | 3.465(1) | | Sn3 | 3.465(1) |
| | Sn6 | 3.592(1) | | Sn6 | 3.564(1) |
| | Sn6 | 3.634(1) | | Sn6 | 3.699(1) |
| Sn5- | Sn2 | 2.934(1) | Sn6- | Sn2 | 2.998(1) |
| | Sn1 | 3.143(1) | | Sn6 | 3.029(2) |
| | Nd2 | 3.253(1) | | Nd3 | 3.177(1) |
| | Nd3 | 3.261(1) | | Nd2 | 3.205(1) |
| | Nd1 | 3.280(1) | | Nd4 | 3.255(1) |
| | Nd1 | 3.306(1) | | Nd4 | 3.260(1) |
| | Nd3 | 3.435(1) | | Nd2 | 3.543(1) |
| | Nd1 | 3.568(1) | | Sn4 | 3.564(1) |
| | Sn5 | 3.594(2) | | Sn3 | 3.592(1) |
| | Nd2 | 3.706(1) | | Sn3 | 3.634(1) |
| | | | | Sn4 | 3.699(1) |
| | | | | Nd4 | 3.740(1) |

ized by STRUCTURE-TIDY [17]*. In the case of $La_2Sn_3$ and $Sm_2Sn_3$ the lattice parameters were obtained from least-squares fits of powder patterns, indexed with the aid of LAZY-PULVERIX [18], using the atomic coordinates of $Nd_2Sn_3$. The lattice parameters of the five phases are reported in Table 1.

The heat capacity of the compounds was measured by the semi-adiabatic heat-pulse method, in the range 1.5 to 50 K. Magnetisation data on $La_2Sn_3$ and $Ce_2Sn_3$ were taken on a Quantum Design SQUID magnetometer in the range 1.8 to 300 K and in applied fields up to 70 kOe.

## Results and Discussion

### *Crystal chemistry*

The structure of $Nd_2Sn_3$ was solved in the triclinic, centrosymmetric space group $P\bar{1}$, chosen on the basis of statistical tests and confirmed during the refinement procedure. The crystal data are summarized in Table 2. Table 3 reports atomic coordinates and equivalent isotropic displacement parameters, while interatomic distances are given in Table 4. It is not easy to define the coordination around each atom. The histogram of distances plotted *vs.* d/Σr (d = distance; Σr = sum of the central and surrounding atom radii) [19], does not work well in this case since a sharp gap in the distance distribution is not recognizable. However, with the reasonable compromise of a cut at d/Σr = 1.14 the neodymium and tin atoms have coordination numbers ranging from 11 to 13 and 9 to 12, respectively.

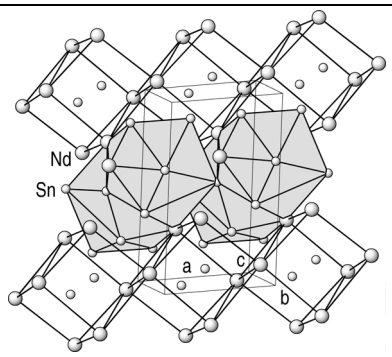


Fig 1. Drawing of the $Nd_2Sn_3$ structure. Two motifs are outlined: pairs of face-linked Nd trigonal prisms centred by Sn6 and sharing an edge of a triangular face, and 11-vertex polyhedra around Nd1 (stippled).

The structure of $Nd_2Sn_3$ is shown in Fig. 1. Pairs of face-linked Nd trigonal prisms, centred by Sn6, share

*Details may be obtained from: Fachinformationszentrum Karlsruhe, D-76344 Eggenstein-Leopoldshafen (Germany) by quoting the Registry No. CSD-412926 (E-mail: crysdata@fiz-karlsruhe.de).

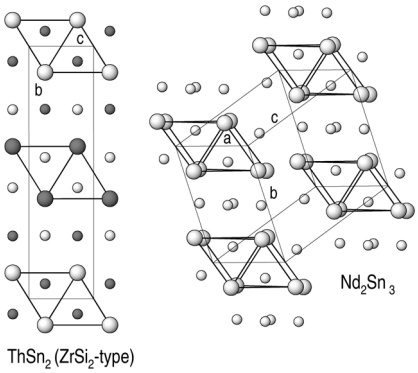


Fig. 2. Comparison of the coordination of part of the tin atoms in $ThSn_2$ and $Nd_2Sn_3$. Large circles: Th or Nd; small circles: Sn. Open and full circles in $ThSn_2$ lie on layers separated by $a/2$. For $Nd_2Sn_3$ all atoms surrounding Sn6 inside the trigonal prisms are shown.

an edge of a triangular face, giving rise to infinite chains along the *a*-axis. The Nd2, Nd3, Nd4 and Sn6 atoms form this motif. In the space left between the chains all other tin atoms and again Nd2 and Nd3 form the coordination polyhedron around Nd1, which is here chosen as the second motif to describe the whole structure. In the figure four of these polyhedra are shown.

Out of the six independent tin atoms, Sn1 and Sn5 have polyhedra of irregular shape: Sn2 is surrounded by a trigonal prism (5Nd+1Sn) centred on the lateral faces by Sn1, Sn6 and Nd1, while a quadrangular prism (5Nd+3Sn) with two faces capped by Sn6 is found around both Sn3 and Sn4.

As can be seen in the right part of Fig. 2, pairs of face-linked Nd trigonal prisms can be drawn, in order to show the environment of the Sn6 atoms inside. Each trigonal prism has two lateral faces capped by Sn2 and another Sn6 atom. Opposite the third lateral face, a square of 2Sn3+2Sn4 at larger distances completes the coordination. It is worth noting that the same coordination is observed in some other rare earth-tin compounds, such as $RSn_2$ phases with R = Gd-Tm, Lu, Y [20], and $ThSn_2$ [21] (all $ZrSi_2$-type), $R_3Sn_7$ and $R_2Sn_5$ (R=La-Nd, Sm) [3] with $Ce_3Sn_7$ and $Ce_2Sn_5$ structure [22], respectively, and $Gd_3Sn_7$ [23]. All these orthorhombic structures can be described as intergrowths of similar segments [24], but different from $Nd_2Sn_3$, their tin-centred trigonal prisms form CrB-like slabs perpendicular to the longest axis. As an example, to show the identical environment of the tin atoms inside the trigonal prisms, a projection of the structure of $ThSn_2$ is reported in the left part of Fig. 2.

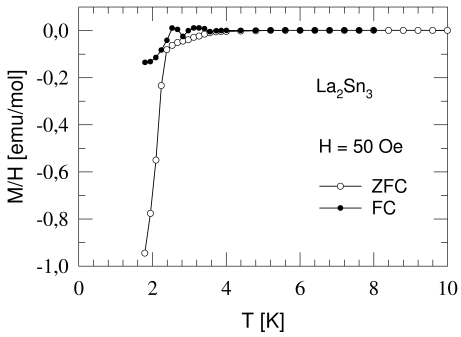


Fig. 3. The zero-field-cooled and field-cooled magnetisation, M/H, of $La_2Sn_3$ in low field of 50 Oe.

*Magnetism*

Fig. 3 shows the magnetisation, M/H, of $La_2Sn_3$ measured below 10 K in a low field of 50 Oe both in zero-field-cooled (ZFC) and field-cooled (FC) modes. For $T > 3.8$ K the susceptibility is paramagnetic with a low value of $\sim 10^{-4}$ emu/mol as expected for a non-magnetic La-compound. The ZFC magnetisation initially becomes slightly diamagnetic below 3.8 K, followed by a huge drop beginning at 2.5 K such that M/H at the lowest temperature of 1.8 K is nearly $-1$ emu/mol. The sharp diamagnetic drop at 2.5 K suggests the possible occurrence of a bulk superconducting transition in $La_2Sn_3$ at that temperature. The appearance of a mild diamagnetic signal at 3.8 K may be due to the presence of some traces of free Sn which is superconducting with a $T_c$ of 3.8 K. The FC magnetisation in 50 Oe is still diamagnetic at the lowest temperature of 1.8 K, due to Meissner expulsion, though considerably reduced (in absolute magnitude) compared to the ZFC value. The slight structure exhibited by FC magnetisation around 3 K may be related to the presence of free Sn as mentioned above.

Fig. 4 shows the inverse magnetic susceptibility of $Ce_2Sn_3$ between 1.8 and 300 K, measured in an applied field of 3 kOe. Above 150 K the inverse susceptibility varies linearly with the temperature following the Curie-Weiss behaviour. From the least squares fitting of the data to the Curie-Weiss expression for the susceptibility $\chi = C/(T - \Theta_p)$, where C is the Curie constant and $\Theta_p$ the paramagnetic Curie temperature, we derive a value of 2.05(5) $\mu_B$/Ce for the effective paramagnetic moment, $\mu_{eff}$, of the Ce ion. $\Theta_p$ is found to be $-22(1)$ K. The value of $\mu_{eff}$ is found to be considerably lower than for the $Ce^{3+}$ free ion value of 2.54 $\mu_B$. Since there are four symmetry in-equivalent Ce ions in

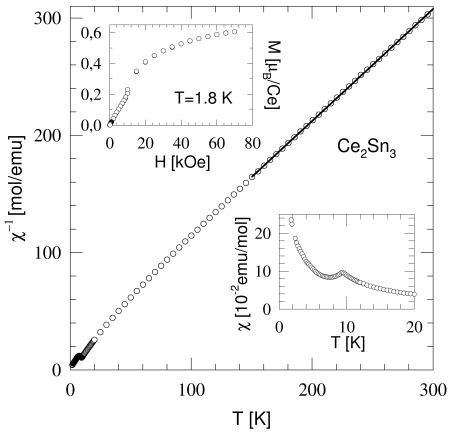


Fig. 4. The inverse susceptibility of $Ce_2Sn_3$ between 1.8 and 300 K. The lower inset shows the susceptibility below 20 K and the upper inset shows the magnetisation at 1.8 K up to 70 kOe.

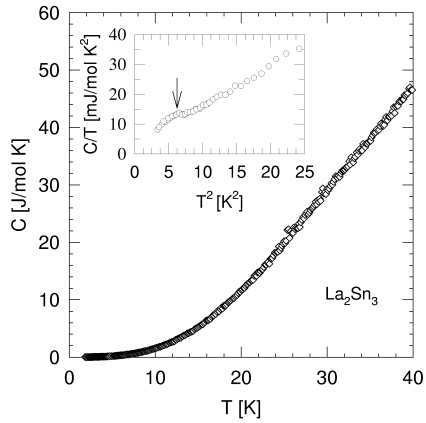


Fig. 5. The heat capacity, C, of $La_2Sn_3$ between 1.8 and 40 K. The inset shows an expanded view of C/T versus $T^2$ below 5 K.

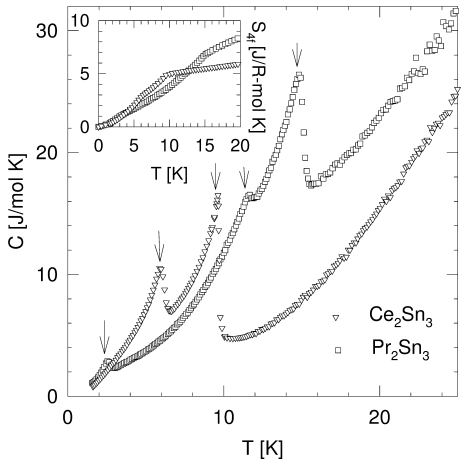


Fig. 6. The heat capacity, C, of $Ce_2Sn_3$ and $Pr_2Sn_3$. The arrows mark the multiple magnetic transitions. The inset shows the corresponding 4f-entropy.

the unit cell the low value of $\mu_{\mathrm{eff}}$ can arise if some Ce ions are not in their trivalent state. But the heat capacity data (discussed below) appear to rule out such a possibility. It is plausible that in the low triclinic symmetry of the structure, the crystal field splitting is larger than 300 K. In that case, a reduced value of $\mu_{\mathrm{eff}}$ will be obtained from the susceptibility data below 300 K. The negative $\Theta_{\mathrm{p}}$ indicates an antiferromagnetic exchange interaction between the cerium ions. The lower inset of Fig. 4 shows the susceptibility *versus* temperature below 20 K. A peak in the susceptibility near $T_N$ = 9.5 K indicates an antiferromagnetic transition. However, the susceptibility increases with temperature at lower temperatures whereas typically in antiferromagnets it decreases down to T = 0 K below $T_N$. Since the heat capacity data (see below) show the presence of a second magnetic transition at 6 K, the observed behaviour of the susceptibility below the peak at 9.5 K may be related either to a spin re-orientation taking place at 6 K or to the magnetic ordering of some Ce ions which do not order magnetically at 9.5 K. The magnetisation at 1.8 K in applied fields up to 70 kOe is shown in the upper inset of Fig. 4. The observed behaviour is in tune with the antiferromagnetic ground state of $Ce_2Sn_3$. The magnetisation shows spin-flop type behaviour near 12 kOe and attains a value of $\sim 0.6\,\mu_{\mathrm{B}}$/Ce at 70 kOe. This low value may also be due to crystal field splitting.

The heat capacity, C, of $La_2Sn_3$ between 1.8 and 40 K is shown in Fig. 5. The inset shows an expanded view of C/T versus $T^2$ below 5 K. An anomaly near 2.5 K, correlated with the onset of strong diamagnetic magnetisation (Fig. 3) is seen in the data. According to the BCS model of superconductivity, the heat capacity at the superconducting transition $T_c$ shows a jump $\Delta_c$ such that $\Delta_c/\gamma T_c$ = 1.43, where $\gamma$ is the Sommerfeld coefficient. Above 3 K the C/T versus $T^2$ exhibits a curvature and the data between 3 and 10 K can be satisfactorily fitted to the expression $C/T = \gamma + \beta T^2 + \delta T^4$ with $\gamma$ = 1 mJ/mol $K^2$. Therefore, a jump of about 1.43 mJ/mol $K^2$ is expected in C/T at the superconducting transition. The anomaly at 2.5 K is similar in magnitude to the theoretically expected value, though it is not sharp. The latter may be due to the width in the superconducting transition which broadens the

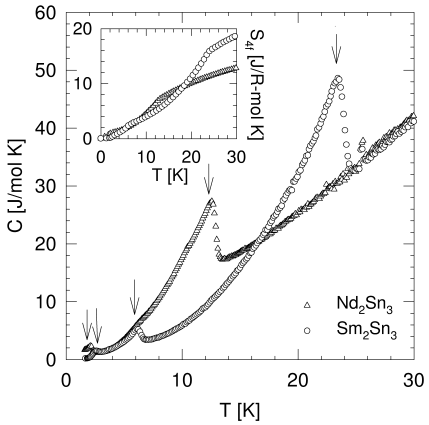


Fig. 7. The heat capacity of $Nd_2Sn_3$ and $Sm_2Sn_3$. The arrows mark the multiple magnetic transitions. The inset shows the corresponding 4f-entropy.

anomaly. Above 3 K the heat capacity of $La_2Sn_3$ increases monotonically with temperature.

The compounds with R = Ce, Pr, Nd and Sm show multiple peaks in the heat capacity data (see Figs. 6 and 7). Their magnitudes indicate that they arise due to the magnetic transitions of magnetic moments associated with the trivalent state of these ions. The multiple transitions may either involve all the four symmetry in-equivalent R-ions ordering at the same temperature and undergoing re-orientations at lower temperatures which is not uncommon in rare earth intermetallics, or they may occur because symmetry in-equivalent R-ions which are ordering magnetically at different temperatures. For example, in $Ce_5Ni_6In_{11}$, cerium ions at 2c and 8k sites order antiferromagnetically at 0.63 and 1.1 K, respectively [25]. The highest transition temperature occurs at nearly 24 K in $Sm_2Sn_3$ which is in accordance with the trend expected on the basis of the deGennes scaling. An estimate of the magnetic entropy was obtained by assuming that the lattice contribution in the magnetic $R_2Sn_3$ compounds is the same as observed in the non-magnetic analogue $La_2Sn_3$ and smoothly extrapolating the data below 1.5 K to 0 K. It is assumed that there are no more magnetic transitions taking place below 1.5 K, which appears reasonable from the value of the heat capacity at the lowest temperature in the magnetic $R_2Sn_3$ compounds. The entropy thus obtained is plotted in the insets of Figs. 6 and 7. For $Ce_2Sn_3$ an entropy of 5.76 J/Ce-mol K, corresponding to crystal field splitting, an S = 1/2 doublet ground state is attained near 15 K, a few degrees above the highest magnetic transition near 10 K. This shows that all the Ce ions are in the trivalent state. In the case of Pr, Nd and Sm compounds the entropy attains the same value below the maximum transition temperature. This indicates either closely spaced crystal field splitting levels at low temperatures which give rise to an effective degeneracy greater than two, or a Schottky contribution from excited crystal field splitting levels.

[1] T. B. Massalski, Binary Alloy Phase Diagrams, ASM International, Metals Park, OH, 2nd Edn. (1990).
[2] F. Weitzer, K. Hiebl, P. Rogl, J. Less-Common Met. **175**, 331 (1991).
[3] F. Weitzer, K. Hiebl, P. Rogl, J. Solid State Chem. **98**, 291 (1992).
[4] A. Palenzona, P. Manfrinetti, M. L. Fornasini, J. Alloys Compd. **280**, 211 (1998).
[5] P. Manfrinetti, D. Mazzone, A. Palenzona, J. Alloys Compd. **284**, L1 (1999).
[6] V. N. Eremenko, M. V. Bulanova, P. S. Martsenyuk, V. E. Listovnichii, Dopov. Akad. Nauk Ukr. RSR, B **9**, 35 (1988).
[7] G. Borzone, A. Borsese, R. Ferro, J. Less-Common Met. **85**, 195 (1982).
[8] E. Franceschi, G. A. Costa, J. Therm. Anal. **34**, 451 (1988).
[9] M. L. Fornasini, F. Merlo, Atti Accad. Naz. Lincei, Rend. Cl. Sci. Fis. Mat. Nat. **50**, 186 (1971).
[10] V. N. Eremenko, M. V. Bulanova, V. E. Listovnichii, V. M. Petyukh, Ukr. Khim. Zh. **54**, 787 (1988).
[11] V. N. Eremenko, M. V. Bulanova, P. S. Martsenyuk, V. E. Listovnichii, Ukr. Khim. Zh. **54**, 1240 (1988).
[12] R. Vogel, T. Heumann, Z. Metallkd. **35**, 29 (1943).
[13] A. F. Ruggiero, G. L. Olcese, Atti Accad. Naz. Lincei, Rend. Cl. Sci. Fis. Mat. Nat. **37**, 169 (1964).
[14] A. Percheron, Colloq. Int. CNRS, 'Les Elements des Terres Rares', Paris-Grenoble, May 5 – 10, 1969, CNRS, Paris, Vol. 1, p. 165 (1970).
[15] A. Altomare, G. Cascarano, C. Giacovazzo, A. Guagliardi, M. C. Burla, G. Polidori, M. Camalli, J. Appl. Crystallogr. **27**, 435 (1994).
[16] G. M. Sheldrick, SHELXL-97, Program for refinement of crystal structures. University of Göttingen, Germany (1997).
[17] L. M. Gelato, E. Parthé, J. Appl. Crystallogr. **20**, 139 (1987).
[18] K. Yvon, W. Jeitschko, E. Parthé, J. Appl. Crystallogr. **10**, 73 (1977).
[19] G. Bruzzone, M. L. Fornasini, F. Merlo, J. Less-Common Met. **22**, 253 (1970).

[20] A. Iandelli, A. Palenzona, Atti Accad. Naz. Lincei Rend. Cl. Sci. Fis. Mat. Nat. **40**, 623 (1966).
[21] S. Cirafici, A. Palenzona, P. Manfrinetti, J. Less-Common Met. **90**, 49 (1983).
[22] J. X. Boucherle, F. Givord, P. Lejay, J. Schweizer, A. Stunault, Acta Crystallogr. **B44**, 377 (1988).
[23] R. V. Skolozdra, L. G. Aksel'rud, V. K. Pecharskii, O. E. Koretskaya, Dokl. Akad. Nauk USSR Ser. B, **12**, 51 (1986).
[24] M. Pani, M. L. Fornasini, Z. Kristallogr. **190**, 127 (1990).
[25] J. Tang, K. A. Gschneidner (Jr.), S. J. White, M. R. Roser, T. J. Goodwin, L. R. Corruccini, Phys. Rev. B **52**, 7328 (1995).